Supplementary Materials for

Molecular Basis of Tubulin Transport within the Cilium by IFT74 and IFT81

Sagar Bhogaraju[1], Lukas Cajanek[2], Cécile Fort[3], Thierry Blisnick[3], Kristina Weber[1], Michael Taschner[1], Naoko Mizuno[1], Stefan Lamla[4], Philippe Bastin[3], Erich A. Nigg[2] and Esben Lorentzen[1]*

correspondence to: lorentze@biochem.mpg.de

This PDF file includes:

Other Supplementary Materials for this manuscript includes the following:

Materials and Methods

Purification and reconstitution of IFT-B complexes

For purification of the *C.reinhardtii* IFT81ΔN/74ΔN/His_6-27/25ΔC complex, insect cells (HighFive, Invitrogen) were infected with baculovirus expressing the complex and grown for 72hours. Extract preparation was carried out as described previously (*24*), and the complex purified using a combination of Ni-NTA, ion-exchange (monoQ column) and size exclusion chromatography. Purification of the IFT70/IFT52/IFT46 complex from *E.coli* was performed as described previously (*24*). Reconstitution of the heptameric IFT81ΔN/74ΔN/70/52/46/His_6-27/25ΔC complex was achieved by mixing equimolar amounts of the IFT81ΔN/74ΔN/His_6-27/25ΔC complex and the IFT70/52/46 complex, followed by Superose6 size exclusion chromatography after an incubation at 4°C for 3hours.

Protein purification and crystallization

His tagged CrIFT81 (residues 1-126) was expressed in *E.coli* BL21 (DE3) GOLD pLysS strain and lysed by sonication in a buffer containing 50mM Tris pH 7.5, 150mM NaCl and 10% glycerol. The protein was purified by Ni-NTA affinity chromatography followed by TEV cleavage to remove the His tag and size exclusion chromatography in a buffer of 10mM HEPES pH 7.5, 150mM NaCl using a superdex 75 or 200 column. CrIFT81N was concentrated to 20mg/ml and crystallized by vapor diffusion. Crystals of CrIFT81N appeared in 0.8M $(NH_4)_2SO_4$, 0.1 M Tris pH 8.0 precipitant condition (Figure S3C). HsIFT81N was purified using the same procedure. Point mutants of HsIFT81N were made using the Quikchange site directed mutagenesis protocol from Agilent Technologies® and all the mutants were expressed and purified like the WT protein. The

IFT81/74_CC complex was produced by co-expression of His_6-HsIFT81 (residues 1-215) and His_6-HsIFT74 (residues 1-272) in the *E.coli* strain BL21 (DE3) GOLD pLysS. Cells were lysed and the proteins were purified using the same procedure as described above.

X-ray diffraction data collection and structure determination

Crystals of CrIFT81N were flash cooled in liquid nitrogen in mother liquor supplemented with 25% glycerol as a cryoprotectant. Diffraction data were collected at the Swiss light source (SLS, Villigen, Switzerland) and processed with the XDS package (*25*). Single wavelength anomalous dispersion X-ray diffraction data were collected from tantalum bromide (Ta_6Br_{12}) soaked and experimental phases calculated using the PHENIX package (*26*). The program BUCCANEER (*27*) was used to automatically build ~80% of the CrIFT81N structure. The model was completed by iterative cycles of manual model building in the program COOT (*28*) and refinement in PHENIX. The obtained structure from the Ta_6Br_{12} soak was then used as a search model for molecular replacement with native data.

MT co-sedimentation assays

99% pure bovine brain tubulin was obtained from Cytoskeleton® and MT were polymerized according to the manufacturers instructions. For co-sedimentation experiments, 3µM of MTs were pre-incubated with 3µM of protein (HsIFT81N or HsIFT74/81_CC) at room temperature for 30min in BRB80 buffer (80mM Pipes-KOH pH 6.8, 1mM EGTA, 2mM $MgCl_2$) supplemented with 20µM taxol to a final reaction volume of 50µL. This reaction mixture was pipetted onto 100µL of cushion buffer (50%

glycerol, 80mM Pipes-KOH pH 6.8, 2mM $MgCl_2$, 1mM EGTA) supplemented with 20μM taxol. The resulting solution was centrifuged at 40.000rpm for 30min in a Beckmann TLA100 rotor. Supernatants and pellets were analyzed using SDS-PAGE followed by coomassie staining.

Electron microscopy

Taxol-stabilized MTs at a concentration of 5μM were mixed with 1.5μM of GST-HsIFT81N or HsIFT74/81_CC in 50 μL of BRB80 buffer. The mixture was incubated for 30 BRB80min at room temperature and 5μL of this reaction mix were placed onto a glow discharged EM grid followed by 2-3 rounds of washing with BRB80 buffer. The sample was stained using 1% Uranyl acetate solution. Images were collected using a FEI-CM200 microscope operating at 160kV at 38,000X magnification corresponding to a pixel size of 2.78Å.

Tubulin co-precipitation assays

3μM of tubulin and 10μM of GST tagged proteins were mixed in 100μL of BRB80 buffer and incubated on ice for 30min. The reaction mixture was then added to 15μL of pre-blocked GSH beads and incubated on a shaker for 1hour at 4°C. The beads were washed extensively with the BRB80 buffer and the proteins bound to GSH beads were eluted with 30mM glutathione and analyzed by SDS-PAGE.

Microscale thermophoresis (MST)

Bovine tubulin was labeled on lysine side-chains using the Cy3 protein labeling kit from Jena Bioscience according to the manufacturers instructions. The average number of lysines labeled per αβ-tubulin dimer was estimated to be 3.6. 200nM of labeled tubulin was titrated with 0.03-2000μM of HsIFT81N or HsIFT81Nmut1 in a total volume of 20μL and 10-16 thermophoresis measurements recorded. Each sample was incubated at room temperature for 10min before measurement. For the HsIFT81/74_CC complex, a lower concentration of 0.003-200μM was used. Thermophoresis measurements were carried out using the NanoTemper Monolith NT.115 instrument (NanoTemper Technologies GmbH) using 50% LED and 65% laser power with the laser on for 40sec followed by an off period of 10sec. The resulting raw data were analysed using the NanoTemper software to obtain binding curves and Kds were calculated using Prism (GraphPad Software).

Subitlisin treatment of tubulin/microtubules

8μM of preformed and taxol stabilized MTs were mixed with 1.25μM of subtilisin in BRB80 buffer containing 20μM taxol in a total volume of 50μL. This reaction mixture was incubated at 30°C for 30min and the proteolysis stopped by adding 1mM PMSF. Proteolysed MTs were spun at 40.000rpm for 30min in a Beckmann TLA100 rotor and the pellet re-dissolved in BRB80 buffer supplemented with 20μM taxol. For the subtilisin treatment of soluble tubulin, 25μM of tubulin were mixed with 1.25μM of subtilisin in a total volume of 120μL of BRB80 buffer. The solution was divided into two equal halves, which were incubated at 30°C for 30min or 120min, respectively, followed by inactivation of the protease by the addition of 1mM PMSF. Untreated and subtilisin

treated tubulin were purified using size exclusion chromatography (superdex 200 column) as shown in Fig. S5A.

Cell culture and transfections

The RPE-1 and U2OS cells were cultured as previously described (*29*). For transient gene expression, cells were transfected with TransIT-LT1 (Mirus) according manufacturers instructions with pcDNA3.1-IFT81 full length (F.L.) and pcDNA3.1-IFT81ΔN (human IFT81 sequences). For the rescue experiments, RNAi resistant plasmid was generated by making silent mutations in the siRNA spanning regions of *IFT81* gene and subsequent cloning of this construct into the pcDNA5.1 vector. This RNAi resistant pcDNA5.1-IFT81 F.L. plasmid was further used to generate rescue plasmids with point and deletion mutations (mut^1, mut^2 and ΔN). For rescue experiments, RPE-1 cells were first transfected with control (GL2) or IFT81 siRNA (target sequence: GGATATCAGTGCAATGGAA and CAGCTCATTAAGAGAGTTGAA, each at 50μM) using Oligofectamine (Invitrogen) according manufacturers recommendations. Cells were subsequently nucleofected with pcDNA5.1-IFT81 (F.L., mut1, mut2 or ΔN) rescue plasmids using Amaxa 4D-Nucleofector (Lonza) and the DS137 program, 48h after the siRNA transfection. Following the plasmid transfection, the formation of primary cilia in RPE-1 cells was induced either by 0.5μM Cytochalasin D (Sigma) or by changing into serum-free media for 24h.

Immunofluorescence microscopy

Cells grown on coverslips were washed with PBS and fixed in methanol (-20°C/5min). In case of the detection of acetylated tubulin, cells were cold treated (+4°C/30min) prior the methanol fixation. Blocking, incubation with primary and secondary antibodies, and washing were done as described before (*29*). The following primary and secondary antibodies were used: mouse anti-acetylated tubulin (6-11B-1, Sigma), rabbit anti-Arl13b (17711, Proteintech), mouse anti-Flag (M2, Sigma), rabbit anti-Flag (F7425, Sigma), rat anti-IFT81, goat anti-CAP350 (*30*), rabbit anti-Cep135 (*31*) (both Alexa 647-labeled), rabbit anti-Cep152 (*32*) (Alexa 555-labeled), Alexa 488 anti-mouse, Alexa 488 anti-rabbit, Alexa 555 anti-mouse, Alexa 555 anti-rabbit (all from Invitrogen), and Cy2 anti-rat (Jackson Immuno Research). Direct labeling of primary antibodies was done with the Alexa-antibody labeling kit (Invitrogen). Coverslips were mounted on slides using Glycergel (Dako). Wide-field imaging was performed on a DeltaVision system (Applied Precision) with a 60x/1.2 or 100x/1.4 Apo plan oil immersion objective. Image stacks were taken with a z-distance of 0.2µm, deconvolved (conservative ratio, 3-5 cycles) and projected as maximal intensity image using SoftWoRX (Applied Precision). For cell counts, at least 50 transfected cells per condition and experiment were analyzed for the presence/absence of primary cilia.

Statistical analyses

Statistical analyses (Students t-test, one-way ANOVA with Bonferronis multiple comparison test) were performed using Prism. $p<0.05$ was considered as statistically

significant difference (*), $p<0.01$ (**), $p<0.001$ (***). Results are presented as mean plus standard error of the mean (SEM).

Generation of trypanosome expressing YFP::IFT81 cell lines

All cells used for this work were derived from *T. brucei* strain 427 (procyclic stage) and were cultured in SDM79 medium supplemented with hemin and 10% foetal calf serum. Cell lines expressing unaltered or mutated YFP::IFT81 were obtained after endogenous tagging. The first 500 nucleotides of the *IFT81* gene (Gene DB number Tb927.10.2640) were chemically synthesized (GeneCust, Luxembourg) and cloned in frame with the *YFP* gene within the HindIII and ApaI sites of the p2675 vector (*33*). The construct was linearized within the *IFT81* sequence with the enzyme XcmI and nucleofected (*34*) in wild-type trypanosomes, leading to integration by homologous recombination in the endogenous locus and to expression of the full length coding sequence of IFT81 fused to YFP. Expression of an IFT81-YFP fusion protein of the correct size was confirmed by western blotting with an anti-GFP antibody (Roche) that cross-reacts with YFP. The IFT81 I46D, L47D double-mutant (YFP::IFT81Dm) was generated from the p2675IFT81 plasmid using the Quikchange site directed mutagenesis protocol from Agilent Technologies®. The construct was linearized and transfected, leading to similar expression levels of YFP::IFT81Dm as for unaltered YFT-IFT81 described above.

Life microscopy analysis of trypanosome cells

Trypanosomes were taken from cultures grown at 1.10^7 cells/mL and the expression of YFP::IFT81 or YFP::IFT81DM was observed in live cells using a spinning disk

UltraView Vox microscope equipped with an oil immersion objective (magnification x100 with a 1.4 numerical aperture). Images were acquired using the Volocity software (Perkin Elmer) with an EMCCD camera (ImagEM X2, Hamamatsu) operating in streaming mode. Images were captured with an exposure time of 100ms during 30secs. Images were analysed using the Volocity software and Image J and kymographs were extracted using Quia (*15*).

Supplementary Text

Model for ciliary length control (Fig. 4 and S8)

Intraflagellar transport is known to play a direct role in ciliary length control as partial inhibition of IFT in a *C.reinhardtii* mutant resulted in shorter flagella (*17*). Similarly, partial depletion of the IFT pool results in the formation of shorter flagella in trypanosomes (35). To assess whether the modulation of tubulin transport is another plausible mechanism for controlling cilium length, we used the measured affinity (K_d=0.9μM) to calculate the fraction of IFT complexes bound to αβ-tubulin as a function of tubulin concentration (Fig. 4A). According to this calculation, 90% of IFT complexes have tubulin bound when the cellular concentration of free tubulin is 8μM, whereas only 10% of IFT complexes have tubulin bound at a tubulin concentration of 0.1μM. As the cellular tubulin concentration is estimated to be in the low μM range (*21*), the affinity to IFT74/81 is thus optimal for such a regulatory mechanism. Tubulin is concentrated at the transition zone fibres emanating from the basal body (*36*), a location where IFT protein also concentrate (*37*). Furthermore, tubulin expression is induced at the onset of ciliogenesis followed by a gradual decrease in tubulin concentration during cilium growth (22, *38-41*). This implies that the tubulin-loading of IFT74/81 is maximal during the early stages of ciliogenesis and may decrease as the cilium elongates and the concentration of free tubulin in the cytoplasm is reduced (Fig. 4B and S8). As a result, less tubulin is delivered to the tip of the cilium as it continues to grow. Combined with modulating IFT, this mechanism could provide an additional important control of cilium length.

Further regulation of the IFT of axonemal precursors is likely to occur via post-translational modifications that modulate affinity to the IFT machinery. Tubulin itself is

known to undergo a large number of modifications (*42*), primarily in the acidic C-terminal tail recognized by IFT74, and modifications in this region could thus change binding properties. Recently, the induction of arginine methylation, which is known to affect protein-protein interactions (*43*), was shown to occur during cilia resorption. The methylation pattern was punctate along the length of the cilium, reminiscent of IFT protein staining, indicating that one or more IFT proteins could be methylated (*44*, *45*). Indeed, a protein post-translational modification database (PhosphoSitePlus®) search reveals that human IFT74 is methylated at R51 (*46*). This residue is part of the basic IFT74 N-terminus required for the high affinity tubulin binding by IFT74/81. Methylation of R51 may thus interfere with the function of IFT74 by neutralizing the critical positive charge required for binding to tubulin E-hooks and hence may compromise tubulin transport by the IFT complex. Methylation of IFT81/74 arginines to reduce the affinity for tubulin might thus be a regulatory pathway that is especially active during ciliary resorption, although further studies are required to elucidate its importance.

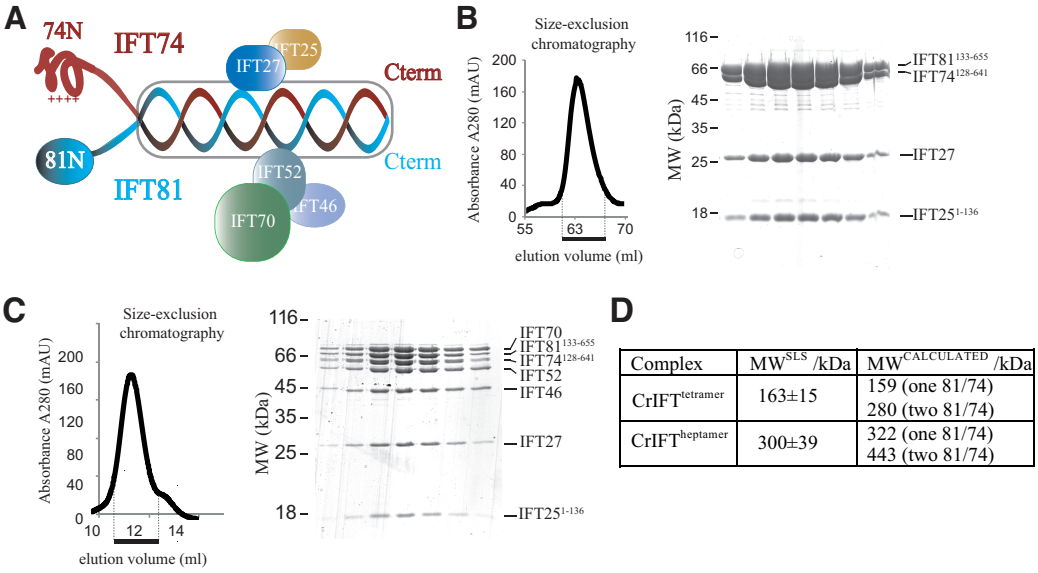

Complex	MW^{SLS} /kDa	$MW^{CALCULATED}$ /kDa
$CrIFT^{tetramer}$	163±15	159 (one 81/74) 280 (two 81/74)
$CrIFT^{heptamer}$	300±39	322 (one 81/74) 443 (two 81/74)

Fig. S1.

(A) Schematics of the IFT-B core complex (not to scale) illustrate that both the IFT25/27 and the IFT46/52/70 sub-complexes associate with the coiled coil regions of IFT74/81. **(B)** Chromatogram from size exclusion purification (left) and associated coomassie-stained SDS-PAGE gel of the indicated peak fraction (right) for purified *C.reinhardtii* IFT25ΔC/27/74ΔN/81ΔN complex lacking the N-terminal regions of IFT74 and IFT81. **(C)** Purification of a heptameric IFT-B core complex obtained by mixing the tetramer shown in (**B**) with a trimeric IFT46/52/70 complex followed by purification using size exclusion chromatography. The results show that IFT74N and IFT81N are dispensable for IFT core complex formation. **(D)** Comparision of the experimentally determined molecular weights with the theoritical molecular weights of $CrIFT^{tetramer}$ (IFT74ΔN, IFT81ΔN, IFT25ΔC and IFT27) and $crIFT^{heptamer}$ (IFT74ΔN, IFT81ΔN, IFT25ΔC, IFT27, IFT70, IFT52 and IFT46). Analysis shows that the molecular weights obtained by static light scattering (SLS) comply with a single copy of both IFT74 and IFT81 in the IFT complex.

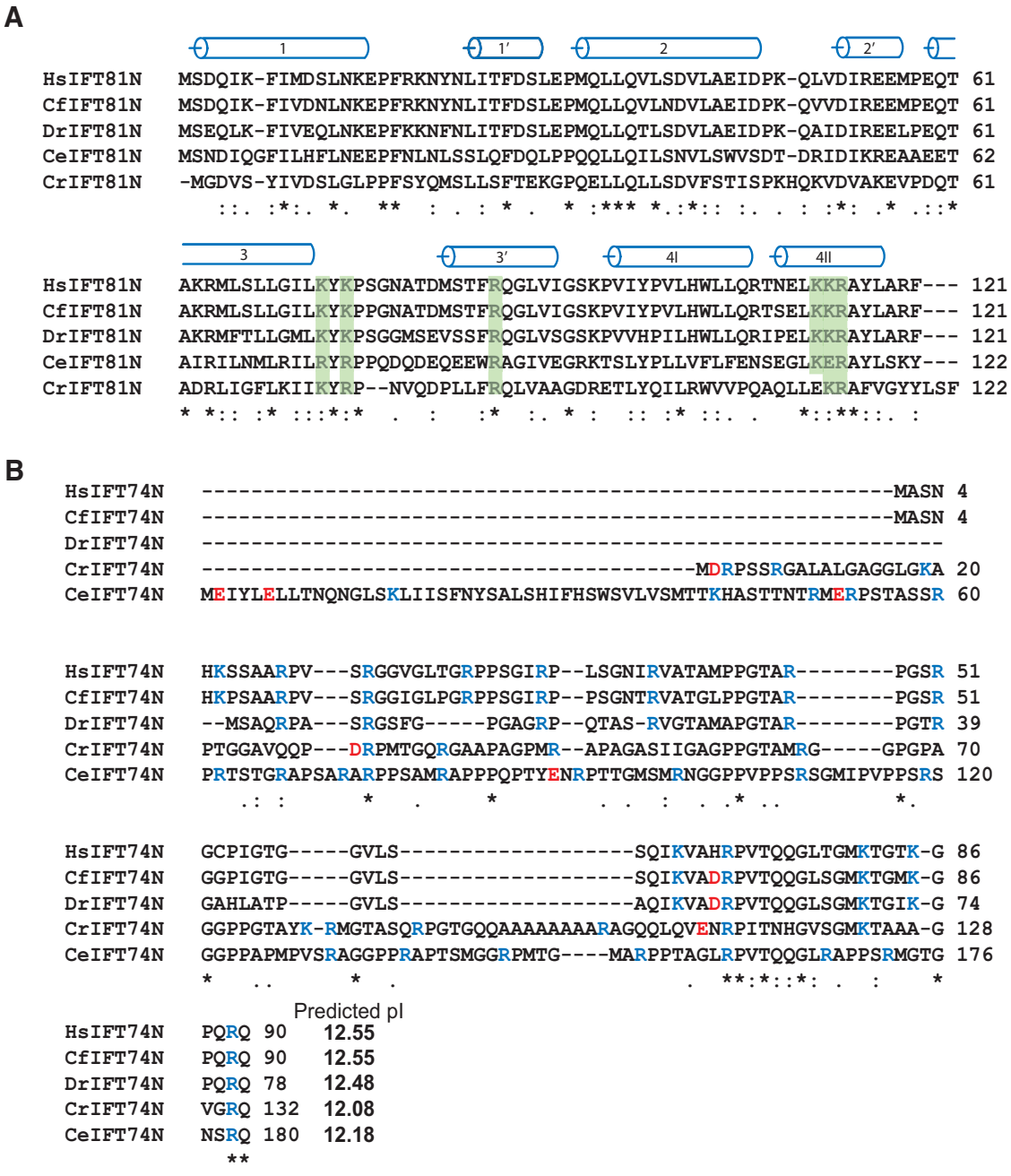

Fig. S2

(A) Sequence alignment of the N-termini of IFT81 proteins from diverse ciliated organisms. Secondary structure elements derived from the CrIFT81N structure are indicated at the top and the conservation of residues are shown at the bottom of the alignment. Functional tubulin binding residues are colored green. **(B)** Sequence alignment of the N-terminal region preceding the predicted coiled-coil domain of IFT74 from different organisms. Conservation is indicated below the sequence. Positively- and negatively-charged residues are shown in blue and red, respectively. The theoretical pIs calculated using the program ProtParam (http://web.expasy.org/protparam/) are indicated.

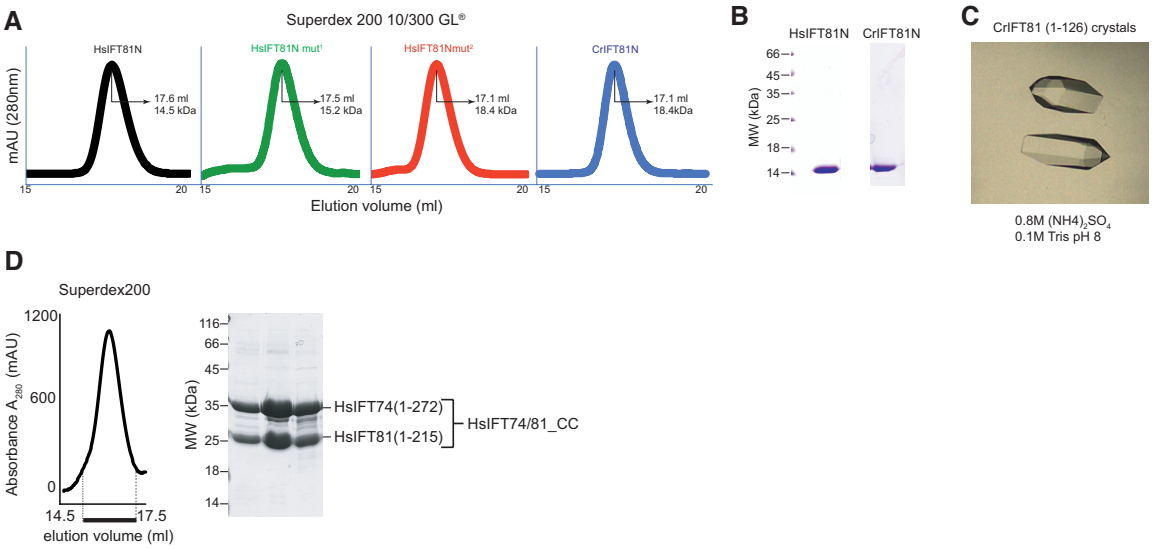

Fig. S3

(A) Size exclusion profiles of IFT81N wild-type and mutant proteins demonstrating that all mutant proteins elute similarly to the wild-type protein and are thus likely to be properly folded. **(B)** Coomassie stained SDS-PAGE gels of purified HsIFT81N and CrIFT81N. **(C)** Hexagonal crystals of CrIFT81N grown by vapor diffusion. **(D)** Purification of truncated HsIFT74/81 complex (HsIFT7481_CC) by size exclusion chromatography. HsIFT7481_CC contains all of the N-terminal domains and a sufficient portion of the coiled-coil domains to form a stable complex.

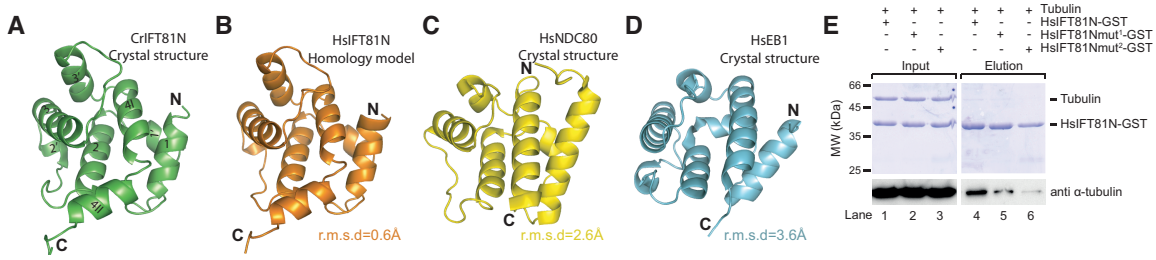

Fig. S4

(A) 2.3Å resolution crystal structure of CrIFT81N shown as a cartoon representation. The termini and α-helices of the domain are labelled. **(B)** Homology model of HsIFT81N based on the crystal structure of CrIFT81N displayed in the same orientation as in panel (A). **(C, D)** Crystal structures of the CH-domains of the MT-binding proteins NDC80 and EB1 after superpositioning onto the CrIFT81N structure shown in **(A)**. **(E)** αβ-tubulin pull-down with wildtype and mutant GST-HsIFT81N proteins. (Top) Coomassie-stained SDS gel of input and eluted proteins. (Bottom) Western-blot using anti α-tubulin antibody to visualize tubulin pulled-down by GST-HsIFT81N. Mutation of conserved basic residues of IFT81N reduces the amount of pulled-down tubulin.

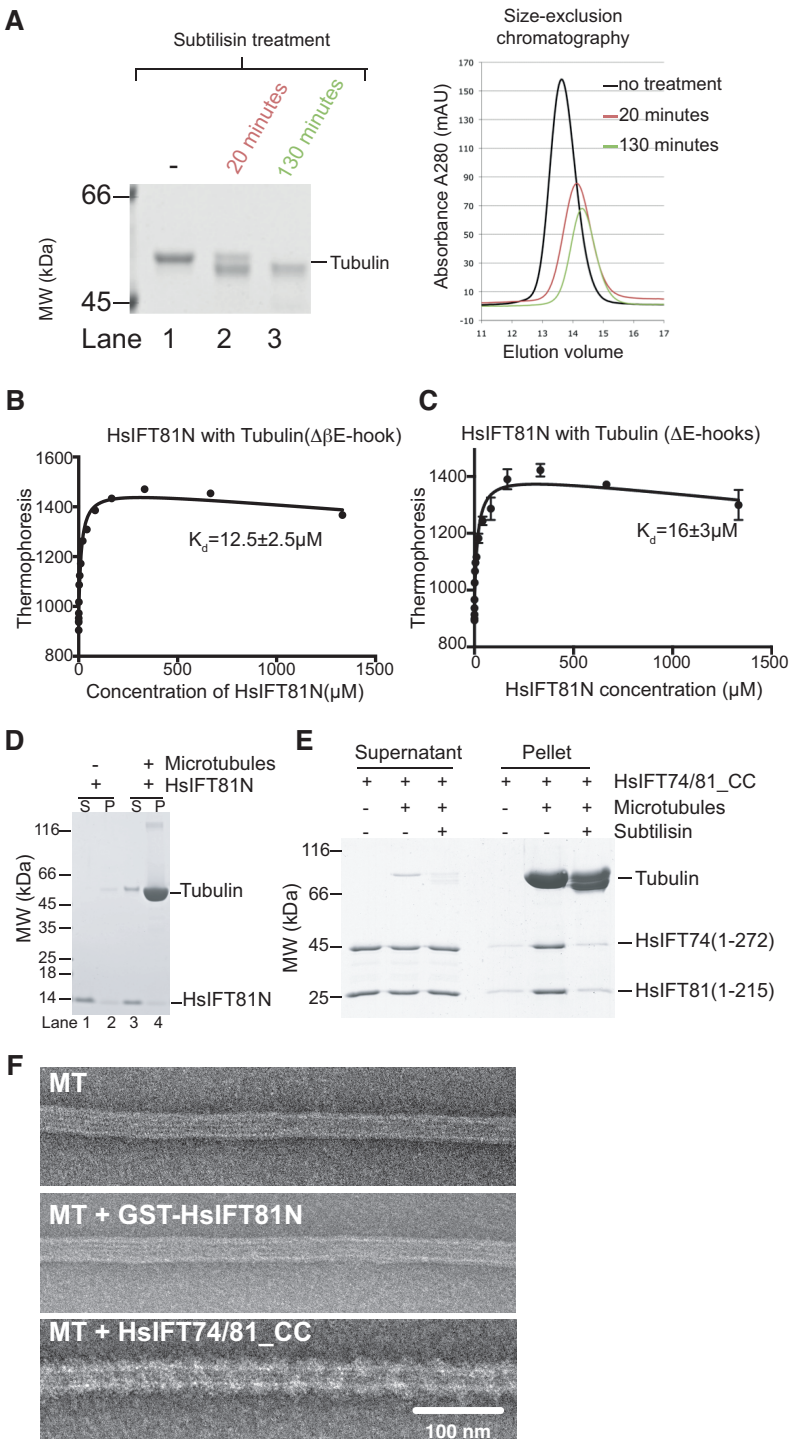

Fig. S5

(A) (left) Coomassie-stained SDS-PAGE gel of subtilisin-protease treated αβ-tubulin to remove the E-hook of β-tubulin (after 20 min) or both α- and β-tubulin (after 130 min). (right) size-exclusion chromatography of proteolysed tubulin **(B)** Microscale

thermophoresis titration of αβ-tubulin lacking the C-terminal tail of β-tubulin (tubulin ΔβE-hook) with HsIFT81N (panel (A), 20 min treatment) showing a similar affinity as for intact αβ-tubulin. **(C)** Microscale thermophoresis titration of αβ-tubulin lacking both the acidic C-terminal tails with HsIFT81N gives a Kd of 16μM. Panels (B) and (C) demonstrate that IFT81N does not required the tubulin E-hooks for interaction. **(D)** MT-sedimentation assay with HsIFT81N and subsequent SDS-PAGE analysis of the supernatant (S) and the pellet (P) reveal only background levels of HsIFT81N co-sedimenting with MT. **(E)** MT-sedimentation experiments where intact αβ-tubulin or tubulin lacking the C-terminal tail of β-tubulin is co-sedimented with the HsIFT74/81_CC complex demonstrates that the high-affinity interaction mediated by IFT74N requires the C-terminal tail of β-tubulin. The concentration of tubulin and HsIFT81N used in the experiments in panels (D) and (E) was 5μM. **(F)** Negative stain EM of taxol stabilized MT incubated with HsIFT81N or HsIFT74/81_CC complex. HsIFT74/81_CC but not HsIFT81N decorates MT. The concentration of tubulin was 1μM and that of IFT81N and HsIFT74/81_CC was 1.5μM.

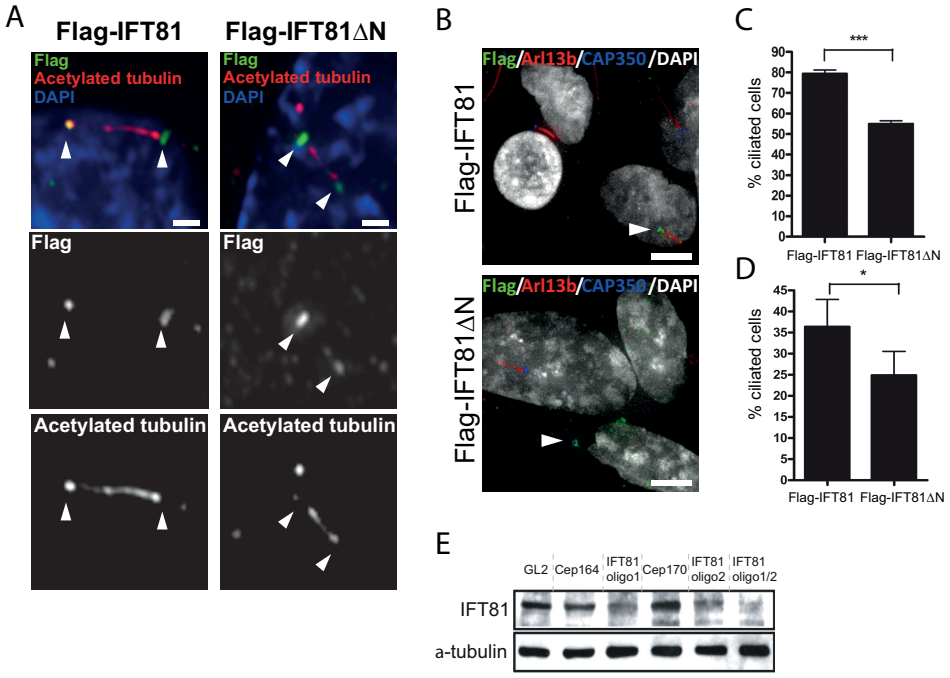

Fig. S6

(A) Both Flag-IFT81 and Flag-IFT81ΔN (in green) are detected at the basal body and the tip of the primary cilium (induced by serum starvation) in RPE1 cells (see the arrowheads). Acetylated tubulin immuno-staining (in red) was used to visualize primary cilia. Scale bar, 1 μm. **(B)** Transient expression of Flag-IFT81ΔN, but not Flag-IFT81 (in green) impairs formation of primary cilia induced by 24h treatment with 0.5μM cytochalasin D in RPE1 cells. Primary cilia were detected by Arl13b immuno-staining (in red), CAP350 (in blue) was used to visualize centrosomes. Arrowheads show Flag positive cells. Scale bar, 5 μm. **(C)** Quantification of the effects of Flag-IFT81 and Flag-IFT81ΔN expression on the presence of primary cilia induced by 0.5μM cytochalasin D. n=3, $p<0.001$(***) by Student's t-test. **(D)** Quantification of the effects of Flag-IFT81 and Flag-IFT81ΔN expression on the presence of primary cilia induced 24h serum starvation. n=4, $p<0.05$(*) by Student's t-test. **(E)** IFT81 siRNA knockdown efficiency was probed by testing the levels of IFT81 protein with anti-IFT81. Transfection of either IFT81 oligo1 or IFT81 oligo2 reduced the protein levels. Combination of oligo1 and oligo2 had the maximum effect on the IFT81 protein levels and hence it was used in the siRNA rescue experiments shown in Fig. 2. Various control RNAi (GL2, Cep164 & Cep170) did not affect IFT81 levels. Levels of α-tubulin in each lane are indicated as a loading control.

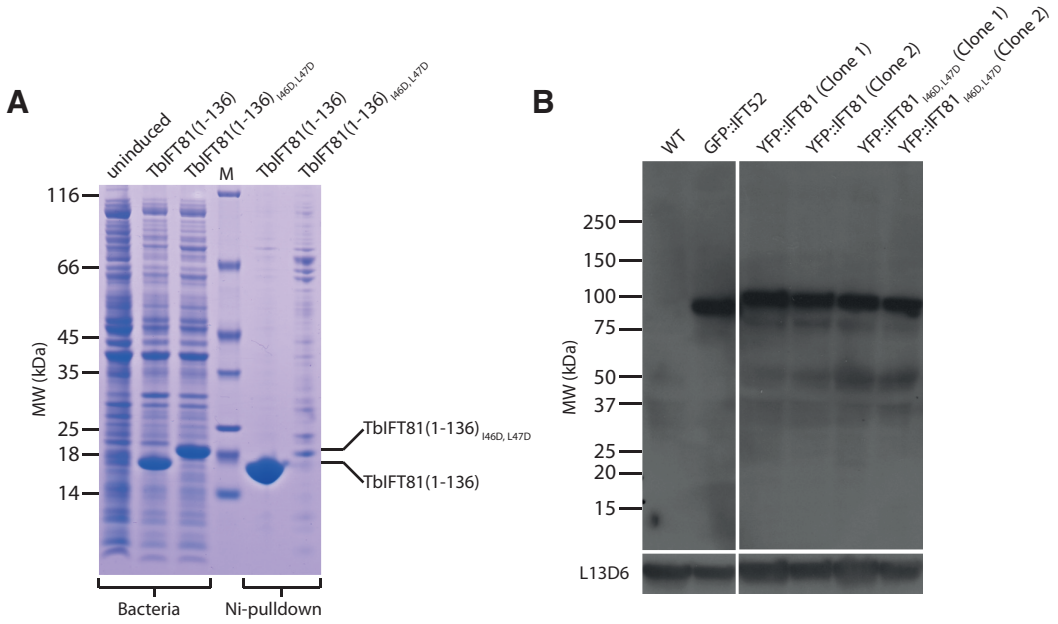

Fig. S7

(A) Expression and Ni-NTA pulldown of His tagged WT and I46D, L47D (Dm) structure-based mutant of *Tryponosma brucei* (Tb) IFT81(1-136). Both proteins are highly expressed as seen from the lanes labeled 'Bacteria'. The 'Ni-pulldown' lanes show that while the WT construct is highly soluble, the mutant solubility is severely compromised indicating that this double mutation disrupts the fold of the N-terminal domain of TbIFT81. **(B)** Western blotting analysis of total protein samples from the Tb cells expressing normal and the mutant (Dm) version of IFT81. 50µg of total protein for each lane are separated on a 4-15% SDS-PAGE and probed with the anti-GFP marker to detect the fusion proteins GFP-IFT52 (*47*), YFP::IFT81 or YFP::IFT81(I46D, L47D). The blot was reprobed with L13D6 to detect paraflagellar rod (PFR) proteins as loading control.

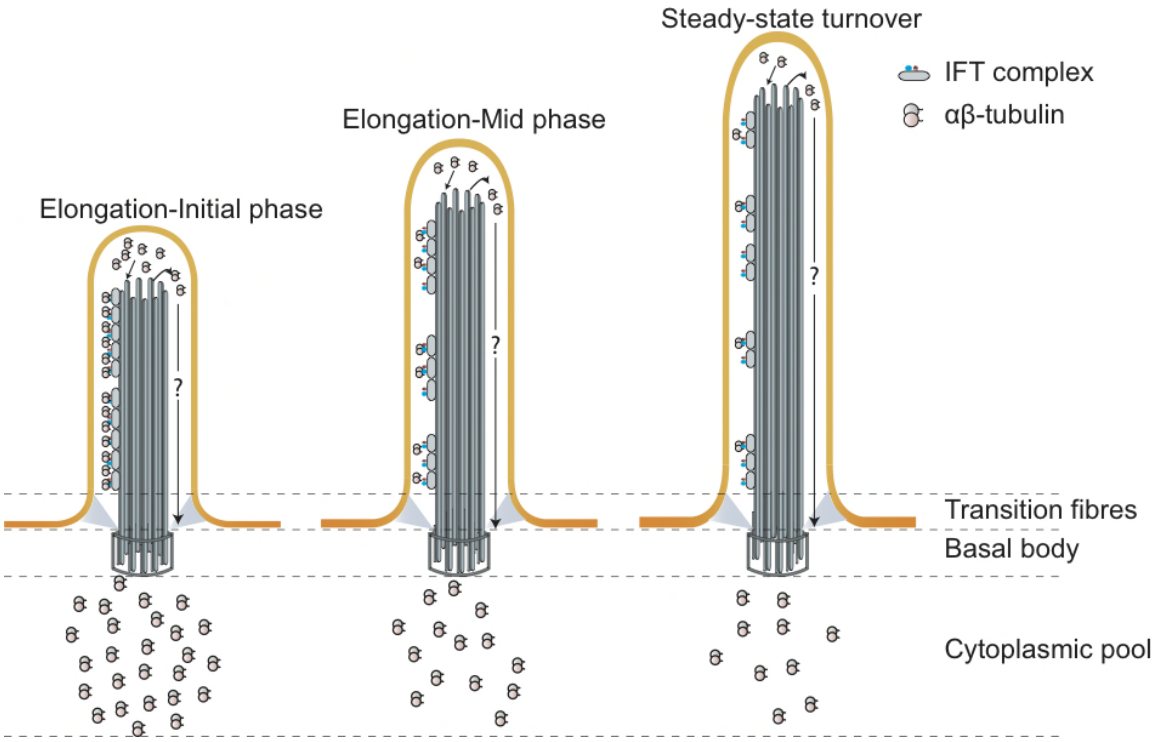

Fig. S8

Model for ciliary length control: 3 representative phases of cilia growth are shown. Each phase is characterized by a varying fraction of IFT complexes bound to tubulin. O_{IFT} is highest in the initial elongation phase and gradually decreases as the cilia approaches its steady state length.

Table S1. Data collection and refinement statistics

	Cr81N_Native	Cr81N_Ta_6Br_{12}
Data collection and scaling		
Wavelength (Å)	0.9793	1.2545
Resolution range (Å)	38 - 2.5 (2.6 - 2.5)	38 - 2.3 (2.4 - 2.3)
Space group	P 6_4 2 2	P 6_4 2 2
Unit cell (Å)	75.1, 75.1, 93.4	76.1 76.1, 94.1
Unique reflections	5727 (869)	13616 (2177)
Multiplicity	12.0 (12.0)	20.1 (20.0)
Completeness (%)	99.5 (96.9)	99.8 (98.1)
Mean I/sigma(I)	21.9 (3.0)	49.2 (12.4)
R-sym	0.05 (0.64)	0.03 (0.20)
Refinement		
Number of reflections	5162	13116
Protein residues	120	124
Number of atoms		
Protein	948	981
Ligands (Ta)	NA	4
Water	0	21
R-work	0.2522 (0.3448)	0.2141 (0.2736)
R-free	0.2854 (0.3657)	0.2391 (0.3218)
Ramachandran favoured (%)	95.6	96.6
Ramachandran outliers (%)	0	0
RMS(bonds)	0.009	0.009
RMS(angles)	1.37	1.30
Average B-factors		
Protein	98.7	57.1
Solvent	NA	57.2

Statistics for the highest-resolution shell are shown in parentheses.

Movie S1 and S2

Movies of WT and Dm mutant IFT81 YFP tagged trypanosome cell lines, respectively.

References

24. M. Taschner, S. Bhogaraju, M. Vetter, M. Morawetz, E. Lorentzen, *J. Biol. Chem.* **286**, 26344–26352 (2011).

25. W. Kabsch, *Acta Cryst.* **66**, 125–132 (2010).

26. P. D. Adams *et al.*, *Acta Cryst.* **66**, 213–221 (2010).

27. K. Cowtan, *Acta Cryst.* **62**, 1002–1011 (2006).

28. P. Emsley, B. Lohkamp, W. G. Scott, K. Cowtan, *Acta Cryst.* **66**, 486–501 (2010).

29. T. I. Schmidt *et al.*, *Current Biol.* **19**, 1005–1011 (2009).

30. X. Yan, R. Habedanck, E. A. Nigg, *Mol. Biol. Cell* **17**, 634–644 (2006).

31. J. Kleylein-Sohn *et al.*, *Dev. Cell* **13**, 190–202 (2007).

32. K. F. Sonnen, L. Schermelleh, H. Leonhardt, E. A. Nigg, *Biology open* **1**, 965–976 (2012).

33. S. Kelly *et al.*, *Mol. Biochem. Parasitol.* **154**, 103–109 (2007).

34. G. Burkard, C. M. Fragoso, I. Roditi, *Mol. Biochem. Parasitol.* **153**, 220–223 (2007).

35. L. Kohl, D. Robinson, P. Bastin, *EMBO J.* **22**, 5336-5346 (2003).

36. A. Stephan, S. Vaughan, M. K. Shaw, K. Gull, P. G. McKean, *Traffic* **8**, 1323–1330 (2007).

37. J. A. Deane, D. G. Cole, E. S. Seeley, D. R. Diener, J. L. Rosenbaum, *Current Biol.* **11**, 1586–1590 (2001).

38. S. D. Guttman, M. A. Gorovsky, *Cell* **17**, 307–317 (1979).

39. D. P. Weeks, P. S. Collis, *Cell* **9**, 15–27 (1976).

40. C. Silflow, *Cell* **24**, 81–88 (1981).

41. V. Stolc, M. P. Samanta, W. Tongprasit, W. F. Marshall, *Proc. Natl. Acad. Sci. U.S.A.* **102**, 3703–3707 (2005).

42. C. Janke, J. C. Bulinski, *Nat Rev Mol. Cell Biol.* **12**, 773–786 (2011).

43. M. T. Bedford, S. G. Clarke, *Mol. Cell* **33**, 1–13 (2009).

44. M. J. Schneider, M. Ulland, R. D. Sloboda, *Mol. Biol. Cell* **19**, 4319–4327 (2008).

45. R. D. Sloboda, L. Howard, *Cell Motil. Cytoskeleton* **66**, 650–660 (2009).

46. P. V. Hornbeck *et al.*, *Nucleic acids research* **40**, D261–D270 (2012).

47. S. Absalon *et al.*, *Mol. Biol. Cell* **19**, 929–944 (2008).